Model development and experimental validation of damage-avoidance structural connections with unbonded post-tensioned prestress

Geoffrey W. RODGERS*, J. Geoffrey CHASE* and John B. MANDER**
*Department of Mechanical Engineering, University of Canterbury, Christchurch 8140, New Zealand
E-mail: geoffrey.rodgers@canterbury.ac.nz
E-mail: geoff.chase@canterbury.ac.nz
**Zachry Department of Civil Engineering, Texas A&M University, College Station, Texas 77843, USA
E-mail: jmander@civil.tamu.edu

Abstract
In the field of earthquake engineering, damage-free structural design methods have received significant research attention in recent years due to the large economic cost associated with sacrificial design methods. In particular, jointed precast concrete and steel connections with unbonded, post-tensioned prestress has been the focus of a significant amount of research. These systems provide controlled inelastic response through gap-opening at the beam-column interface instead of through yielding and damage of the structural elements. The development of a model that captures all the associated characteristics and provides an accurate prediction of response adds significant confidence in response simulations

A time-incremental model of the connection behaviour is developed that accounts for yielding of the prestressing tendons, reduction of the prestressing force, friction between the post-tensioning tendons and the containing ducts, and asymmetry from non-centrally located tendons. The model is formulated using a combination of incremental versions of the Menegotto-Pinto and Ramberg-Osgood type, providing a smooth, continuous loading and unloading approximation to the piecewise linear behaviour. The model is validated against experimental results for an 80% full-scale jointed precast concrete connection with inputs drifts up to 4%. Results show very good agreement with the experimental results, with errors generally less than ±5%. Overall, the model is generalisable to other connections using steel and concrete rocking connections that utilise this type of damage-free design approach and is a useful tool for evaluation of connection designs.

Key words: Unbonded Post-Tensioned Prestress, Damage-Avoidance Design (DAD), Concrete Structures

1. Introduction

Cast insitu reinforced concrete or monolithic precast concrete structures resist earthquake ground motions by dissipating energy in plastic hinge zones located at beam ends adjacent to the beam-column joint. But seismic response can lead to significant damage and degradation at such beam-column connections. The development of precast concrete systems with unbonded post-tensioned prestressed jointed connections that provide dissipative non-linear response due to gap-opening, instead of through structural damage in a plastic hinge zone, has been the focus of recent research[1-4]. Such connections utilising Damage Avoidance Design (DAD) principles[5] typically have low inherent damping.

Structural response for a jointed precast system is a combination of elastic member deflection and rigid body rotation. This study investigates the independent effects of elastic sub-assembly deformation and post-gap opening rigid-body rotation of the structural elements. Previous research has developed simple yet effective models for this type of jointed precast connection which provide good agreement with experimental results[2].

Although this previous research of Li et al.[2] provides a simple explicit model to describe the overall pushover behaviour, the model does not include several aspects of connection performance. While the model incorporates yielding of the prestressing tendons, it does not incorporate the prestress force reduction on subsequent cycles. The previous model provides an upper and lower bound to represent the force contributions due to friction. However, the unloading is based on a signum function and acts as a simple switch which does not capture the initial unloading stiffness due to tendon relaxation. The previous model will likely provide accurate results for jointed precast prestressed connections that utilise straight tendon profiles, and have low inherent friction, if no tendon yield is observed. However, if any notable friction is present or if tendon yield occurs, the model will no longer provide accurate results. Therefore, the modelling presented herein extends this earlier work to incorporate friction in the prestressing system, and changes to subsequent cycles if tendon yield occurs. The model developed moves to a time-incremental form using different loading and unloading stiffness to capture friction and yielding effects.

2. Experimental Investigation

The model developed herein is validated against experimental observations using a full-scale beam-to-column subassembly. The prototype 3D subassembly represents an interior joint of a ten-storey reinforced concrete building[6]. The subassembly consisted of a seismic beam cut at its midpoint (the approximate location of the point of contraflexure) and an orthogonal gravity beam. All beams were 560 mm deep and 400 mm wide, framing into a central 700 mm square column. The orthogonal beam is referred to as the gravity beam, and was designed for one-way precast flooring panels. The other beam is referred to as the seismic beam, designed predominantly for seismic forces. This study investigates the contributions of unbounded post-tensioned prestress to seismic response based on uni-directional testing of the seismic beams. The beam prestress system consisted of two concentric 26.5mm diameter high-strength, high-alloy unbonded and post-tensioned prestressing thread-bars passing through two 45 mm diameter PVC ducts. Detailed photographs, diagrams, and design details can be found in Li[1], Solberg[4] and Rodgers[7].

3. Modelling Connection Behaviour

Overall joint hysteresis for this type of un-bonded post-tensioned prestressed concrete armoured (damage-protected) connections is a combination of elastic member deflection and rigid body rotation. The presence of the unbonded post-tensioned prestress initially delays gap opening. Lateral column deflections in this regime are thus a function of the elastic deformation of structural elements only, until the applied moment at the connection leads to gap opening. This resisting moment is provided by the clamping effect of the prestress within the beam at the column interface. The column shear required for gap opening is therefore a function of the level of prestress provided by the beam tendons.

The column shear and flexural displacements associated with gap-opening deflection can be calculated using beam bending theory and rigid body kinematics. The post gap-opening stiffness remains until the tendon elongation associated with the rigid body component reaches tendon yield. At this point, further column deflection occurs with no further increase in column shear. Any inelastic (plastic) tendon elongation will reduce the initial post-tensioning force on unloading and any subsequent cycles.

3.1 Modelling the Initial Elastic Loading Behavior

Under initial elastic loading both the beam and column deflect without gap-opening at the connection and contribute to the total subassembly displacement. Figure 1 present a schematic diagram of the subassembly showing the associated nomenclature.

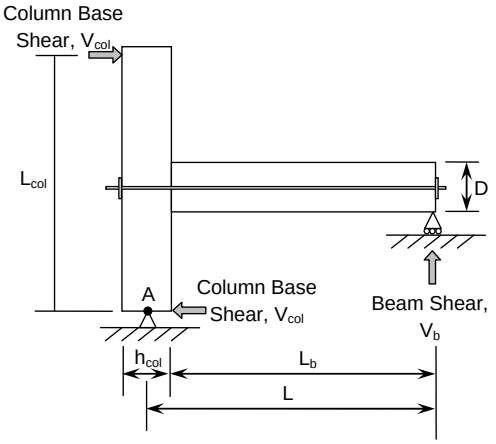

Fig. 1 Beam-column subassembly nomenclature.

During the initial elastic deformation regime the beam and column elastically deflects. The lateral deflection at the top of the column due to both beam and column deflection is defined as Δ_{col} and can be defined in relation to the applied column shear, V_{col}, as:

$$\Delta_{col} = V_{col}\left[\frac{(L_{col}-D)^3}{12EI^*_{col}} + \frac{L^2_{col}L^2_b}{3LEI^*_b}\right] \quad (1)$$

where EI^*_{col} and EI^*_b are the effective column and beam stiffness values. The effective stiffness values have been approximated using moment area methods as 26% of the gross stiffness for uni-directional testing and 14% for bi-directional testing[2]. A detailed derivation of Equation (1) is presented in Rodgers[7].

3.2 Inclusion of Rigid-Body Loading Behavior

Following the elastic deformation regime, the subassembly will undergo rigid-body rotation after gap-opening. This rigid body regime requires additions to the model for the post gap-opening regime and associated mechanics. The combination of pre gap-opening elastic beam deformation, post gap-opening deformation resulting in elastic tendon elongation, and post gap-opening deformation with inelastic (plastic) tendon elongation creates an overall tri-linear response. This overall tri-linear loading path can be calculated based on elastic member deflection and rigid body rotation. Figure 2 presents the tri-linear elasto-plastic backbone curve for monotonic (pushover) behaviour of the subassembly. It includes the pre-gap-opening elastic deflection, and post-gap-opening behaviour, but does not include the effects of friction. Initial elastic deformation of the subassembly prior to gap-opening has stiffness (K_1+K_2). Further elastic beam deflection and rigid body rotation after gap-opening gives stiffness K_2. Finally, the unbonded post-tensioned tendons yield.

In Figure 2, M_{gap} is defined as the connection moment at gap opening. Here Δ_{gap} is the displacement at the top of the column from elastic deformation of the subassembly at gap opening. Further, Δ_{yield} is the displacement of the subassembly from beam deflection at the onset of plastic deformation of the post-tensioned tendons, which occurs at a connection moment of M_{yield}. All of the points shown in Figure 2 can be easily calculated from statics and kinematics, using the subassembly measurements in Figure 1.

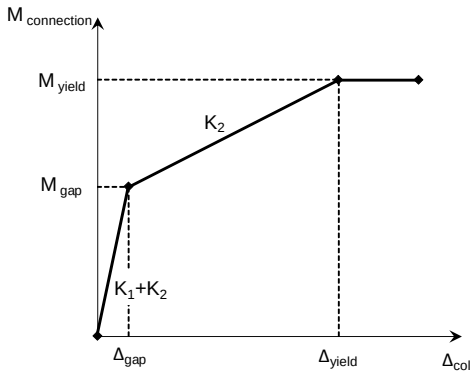

Fig. 2 Bilinear-elastic-plastic monotonic backbone curve of a jointed precast system, where the connection moment is defined $M = V_{col}L_{col}$

The moment produced at the beam-column interface (rocking connection) at gap-opening, M_{gap}, under positive and negative rotations is respectively defined:

$$M_{gap} = F_{PT\_initial}\left(j_{PT}^{\pm}\right)D \tag{2}$$

where $F_{PT\_initial}$ is the total initial tensioning force in the tendons, j_{PT} is the fractional lever-arm of the tendon, the + and – indices refer to rocking about the bottom and top corners of the beam end, respectively, and D is the beam depth. Note that j^{+} and j^{-} are proportional scalars of the beam depth with $j^{+} + j^{-} = 1$.

The displacement at the top of the column due to beam deflection at gap-opening, Δ_{gap}, is defined from the value of connection moment at gap-opening M_{gap} in Equation (2). Equation (1) can be re-written at gap opening using $V_{col,gap} = M_{gap}/L_{col}$:

$$\Delta_{gap} = \frac{M_{gap}}{L_{col}}\left[\frac{(L_{col}-D)^3}{12EI_{col}^{*}} + \frac{L_{col}^2 L_b^2}{3LEI_b^{*}}\right] \tag{3}$$

Moreover, the initial elastic stiffness of the subassembly, (K_1+K_2), as presented in Figure 2, can be calculated using Equations (2) and (3) and is defined:

$$K_1 + K_2 = \frac{L_{col}}{\left[\frac{(L_{col}-D)^3}{12EI_{col}^{*}} + \frac{L_{col}^2 L_b^2}{3LEI_b^{*}}\right]} \tag{4}$$

The connection moment and displacement at tendon yield can be similarly calculated, but occur at the point that plastic strain is induced in the tendons. The connection moment, M_{yield}, is given:

$$M_{yield} = \sigma_{yield} A_{PT}\left(j_{PT}^{\pm}\right)D = F_{PT\_yield}\left(j_{PT}^{\pm}\right)D \tag{5}$$

where σ_{yield} is the yield stress of the tendons, A_{PT} is the total cross-sectional area of the tendons, and F_{PT_yield} is the total force in the tendons at yield.

Finally, the displacement at the top of the column from elastic and rigid body beam deflection at tendon yield, Δ_{yield}, can be defined as a sum of elastic deformation and rigid body deflection components:

$$\Delta_{yield} = \frac{M_{yield}}{L_{col}}\left[\frac{(L_{col}-D)^3}{12EI_{col}^{*}} + \frac{L_{col}^2 L_b^2}{3LEI_b^{*}}\right] + L_{col}\frac{(\varepsilon_{yield}-\varepsilon_{initial})L_t}{\eta\left(j_{PT}^{\pm}\right)D}\frac{L_b}{L} \tag{6}$$

where ε_{yield} is the total tendon strain at the onset of plastic deformation, $\varepsilon_{initial}$ is the initial strain in the tendons from post-tensioning alone before gap opening, L_t is the total length of the unbonded tendon, and η is the number of rocking interfaces spanned by the tendons.

Finally, the value of the post gap-opening stiffness, K_2 can easily be calculated from the geometry in Figure 2, and Equations (2), (3), (5), and (6). The stiffness is defined:

$$K_2 = \frac{\left(j_{PT}^{\pm}\right)D\left(F_{PT,yield} - F_{PT,initial}\right)}{L_{col}\dfrac{(\varepsilon_{yield} - \varepsilon_{initial})L_t}{\eta\left(j_{PT}^{\pm}\right)D}\dfrac{L_b}{L} + \dfrac{\left(j_{PT}^{\pm}\right)D\left(F_{PT,yield} - F_{PT,initial}\right)}{L_{col}}\left[\dfrac{(L_{col}-D)^3}{12EI_{col}^*} + \dfrac{L_{col}^2 L_b^2}{3LEI_b^*}\right]} \quad (7)$$

Note that the terms in the denominator can be segregated into a rigid body component (the first term) and post gap-opening elastic deflection component (the second term). If the elastic stiffness is much higher than the post gap-opening stiffness, then the rigid body component will have the major influence of the denominator.

3.3 Incorporation of Prestress Friction Effects

If the connection utilizes a straight unbounded tendon profile and the duct is of a notably larger diameter than the tendon, it is unlikely any significant friction will exist. However, if a draped or bent tendon profile is utilized, as is commonly done for beams carrying gravity loads and for the seismic beams within this study, then frictional effects will affect cyclic loading performance.

Using the formula for prestress loss effects presented in Li et al.[2] and assuming the product ($\mu_f \alpha_{PS}$) is small so that the higher order terms in the expanded exponential expression can be neglected, the prestress losses due to frictional effects, δF, is defined:

$$\delta F = F_{PT1} - F_{PT2} = \mu_f \alpha_{PS} F_{PT1} \quad (8)$$

where μ_f = angular coefficient of friction; and α_{ps} = the angle change of the tendon (in radians); F_{PT2} = the prestress force at the joint face; and F_{PT1} = the applied jacking force to the prestress system. Note that this equation is an approximation of the force differential that exists within the tendon due to friction between the tendon and the duct it is located in.

Figure 3 presents the effect of friction on the monotonic pushover behaviour. The gap-opening resistance increases. Under cyclic loading, the stiffness changes due to frictional effects. By considering the mechanics of the connection, it is evident that the presence of friction within the tendon-duct system will affect the force in the tendon across the beam-column interface. A force differential will be present in the tendon where it contacts the duct. Upon reversal the tendon will elastically relax before a force differential of an opposite sign exists. The elastic relaxation in the tendon during changes of direction results in a stiffness, K_{fr}, as shown in Figure 3, rather than a vertical force discontinuity, as predicted by models utilising a signum function on the velocity to define to friction force[2].

The elastic components are now defined as ($K_1 + K_2^+$) for loading, and ($K_1 + K_2^-$) for unloading, with the post-gap opening stiffness defined:

$$K_2^+ = K_{2\_nom}\left(1 + \mu_f \alpha_{PS}\right) \quad (9a)$$

$$K_2^+ = K_{2\_nom}\left(1 + \mu_f \alpha_{PS}\right) \quad (9b)$$

where K_{2_nom} is the nominal post-gap opening stiffness, K_2, without any friction modification, as defined in Equation (7), and shown in Figure 2. The intersection of the different K_2 lines on the horizontal axis, Δ_o, is the effective origin for the post-gap opening regime. If no initial post-tensioning was present, then the initial elastic loading branch would not exist, and Δ_o would move to the axes origin, such that $\Delta_o = 0$.

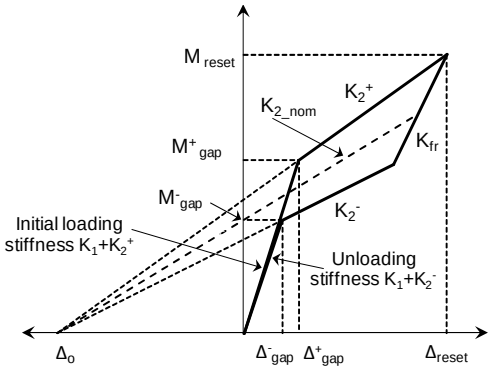

Fig. 3 Schematic representation of the loading regime with the addition of friction. The dashed line labelled K_{2_nom} represents the post-gap opening stiffness without friction.

3.4 Loading Stiffness Definition

To computationally model this piece-wise linear behavior in a smooth continuous sense, differential versions of the Menegotto-Pinto[8] and Ramberg-Osgood[9] equations are used. To capture all of the different regimes in the response of Figure 3, it is necessary to develop different stiffnesses for the loading and unloading behaviour. The overall loading stiffness, $K^{+}(\Delta)$, has three different regions, as shown in Figure 3, and is defined:

$$K^{+}(\Delta) = K_1^{*+}(\Delta) + K_2^{*+}(\Delta) \tag{10}$$

where $K_1^{*+}(\Delta)$ is defined using a differential version of the Menegotto-Pinto equation:

$$K_1^{*+}(\Delta) = \frac{K_1}{\left\{1 + \left|\frac{M_{reset} + (K_1 + K_2^{+})(\Delta - \Delta_{reset})}{K_2^{+}(\Delta - \Delta_o)}\right|^{R_P}\right\}^{(1/R_P+1)}} \tag{11}$$

where M_{reset} = the connection moment at the beginning of loading, and Δ_{reset} = the input displacement at the beginning of loading. Note that for a cycle that begins at the origin (0,0) then $M_{reset} = 0$, and $\Delta_{reset} = 0$. The denominator term goes to 1.0 and $K_1^{*+}(\Delta)$ goes to K_1 when $M_{reset} + (K_1 + K_2^{+})(\Delta - \Delta_{reset}) < K_2^{+}(\Delta - \Delta_o)$. The denominator goes to infinity, and K_1^{*+} goes to 0, when $M_{reset} + (K_1 + K_2^{+})(\Delta - \Delta_{reset}) > K_2^{+}(\Delta - \Delta_o)$. The rate of change of the denominator at the transition is defined by the value of R_p. For large values (R_p >> 1.0), the transition is very sharp, approximating the change seen in Figure 3. For lower values ($R_p \approx$ 2-5), the transition is more gradual. The slower transition in stiffness induces a more rounded transition in the overall model response.

The stiffness component $K_2^{*+}(\Delta)$ should be active when the connection moment is less than that which corresponds to tendon yield and is defined:

$$K_2^{*+}(\Delta) = \frac{K_2^{+}}{1 + (R_Y - 1)\left|\frac{M_{i-1}}{M_{yield}}\right|^{(R_y - 1)}} \tag{12}$$

where the value of the exponent, R_y, defines the rate of change of the gradient transition as the yield point is approached, using a Ramberg-Osgood type of formulation. For large values of R_y, the transition is very sharp, approximating the change seen in Figure 3. For lower values the transition is more gradual.

3.5 Unloading Stiffness Definition

To capture the different regimes in the unloading response of the model it is necessary to develop a stiffness definition for the unloading behaviour similar to that used for loading. Similar to the loading path, the overall unloading stiffness, $K^{-}(\Delta)$, has three different regions, as shown in Figure 3.

The required stiffness as a function of the input displacement is defined as $K^{-}(\Delta)$. A line that determines the friction slope, K_{fr}, is defined relative to the reset point, using a similar approach to that utilised for loading in Equation (11).

From these observations, the unloading stiffness, $K^{*}(\Delta)$, is defined:

$$K^{-}(\Delta) = K_1^{*-}(\Delta) + K_{fr} + K_2^{*-}(\Delta) \tag{13}$$

where the K_{fr} term is always present, and is not dependent on any response parameters. The $K_1^{*-}(\Delta)$ and $K_2^{*-}(\Delta)$ components are defined:

$$K_1^{*-}(\Delta) = \frac{K_1}{\left\{1 + \left|\frac{K_1\Delta}{-K_2^{-}\Delta_o}\right|^{R_P}\right\}^{(1/R_P+1)}} \tag{14}$$

$$K_2^{*-}(\Delta) = \frac{\left(K_2^{-} - K_{fr}\right)}{\left\{1 + \left|\frac{\left\langle M_{reset} + K_{fr}(\Delta - \Delta_{reset})\right\rangle}{K_2^{-}(\Delta - \Delta_o)}\right|^{R_{fr}}\right\}^{(1/R_{fr}+1)}} \tag{15}$$

where the McCauley's brackets term, indicated by $\langle\ \rangle$ is defined as $\langle A\rangle = A$ if $A > 0$, and $\langle A\rangle = 0$ if $A \le 0$ for any value of input A. Thus, they are similar to the well-known Heaviside function. A detailed derivation of Equations (13)-(15) can be found in Rodgers[7].

3.6 Calculating Δ_o

The equations describing stiffness can be considered a beam-column-tendon model relating positive displacements to the connection moment. Although negative values will be present at the interface due to reversed loading, a positive value is maintained, and the sign of the lever-arm term for the tendons, $(jD)_{PT}^{\pm}$, is utilized to correct for the associated directional dependence.

The initial value of the connection moment at gap opening, M_{gap} can be calculated based on the observed initial prestressing force, and using Equation (2). From this calculated value the origin of the K_2^{+} and K_2^{-} lines, Δ_o (as defined in Figure 3) can be calculated from the geometry as:

$$\Delta_o = \frac{-K_1}{K_{2\_nom}\left(K_1 + K_{2\_nom}\right)} M_{gap} \tag{16}$$

where K_2 = the nominal post gap-opening stiffness without modification for friction, as labelled in Figures 2 and 3.

3.7 Yielding Effects and Prestress Force Reduction

Although the model currently accounts for yielding within a response cycle due to the tri-linear behaviour, the model must also account for the prestress force reduction on unloading and on subsequent cycles. Any inelastic tendon elongation will result in a decrease in prestress force and therefore alter the behaviour on unloading and any

subsequent cycles. This reduction represents a shift in the location of the origin of the K_2^+ and K_2^- lines, Δ_o. The location of Δ_o changes by the amount of inelastic tendon elongation, and relocates to $\Delta_{o,new}$.

The modification to the value of Δ_o can be easily calculated based on the new K_2^+ line that originates at $\Delta_{o,new}$ and intersects the reset point. It should also be noted that this K_2^+ line is the re-loading path for subsequent cycles. The value of $\Delta_{o,new}$ is defined:

$$\Delta_{o,new} = \Delta_{reset} - \frac{M_{reset}}{K_2^+} \tag{17}$$

Equation (17) must only be implemented on a reset (when the loading direction changes – ie: the sign of the velocity changes) and only when tendon yield has also occurred (when $\Delta_{reset} > (\Delta_o + M_{yield} / K_2^+)$).

4. Overall Connection Modelling

The approach presented has been formulated as a subassembly model where the connection moment and displacement are always positive. The subassembly model can be considered to be formulated to give the connection moment for a normalized value of lever-arm, jD, where the fractional lever-arm, j = 1.0. The beam model will always yield positive moments, but the inclusion of the directionally dependent multiplier j corrects for the sign, providing the overall connection behaviour for both positive and negative connection displacements.

The connection moment at gap opening is linearly proportional to the magnitude of j. However, the post-gap opening stiffness is approximately proportional to the square of the magnitude of the fractional lever-arm, j. This quadratic relationship is explained by considering the underlying kinematics. Compared to a nominal value of fractional lever-arm, j, halving the magnitude will induce only half of the displacement in the tendon, and therefore result in only the half the increase in tendon force. Furthermore, this increase in force will only contribute half of the moment to the connection, due to the smaller lever arm, providing in combination the quadratic relationship.

Figure 4 presents the schematic model response for two different values of j. Considering the geometry of the model response, it is evident in Figure 4 that the location of the origin of the K_2 lines, defined as Δ_o, is dependent on the value of the fractional lever-arm, j. The K_2 line must intersect the ($K_1 + K_2^+$) at a location linearly proportional to the value of j but with a slope approximately quadratically proportional to magnitude of j. Therefore, the location of Δ_o will be approximately inversely proportional to magnitude of j.

Under full cyclic loading the model must incorporate connection behaviour for both positive and negative rotations in the presence of prestressing tendons that are not centrally located ($j^+ \neq j^-$) with respect to the beam centreline. Under these conditions, the model parameters, M_{gap}, M_{yield}, K_2 and Δ_o are all directionally dependent, as they are all a function of the fractional lever-arm, j, as defined in Equations (2), (5), (7), and (15), respectively. To accommodate this directional dependence, the values need to be switched based on the direction of loading, and the associated value of either j_{PT}^+ or j_{PT}^-. However, all other model equations hold given this switching to account for the directional response behaviour.

This switching can be readily implemented a number of ways, including: 1) using conditional statements, or 2) incorporating a switching function using Heaviside functions, sigmoid functions, or hyperbolic tangents. The implementation is straightforward computationally and only requires that the values be assigned at any change in the sign of the input displacement. Note that the directional dependence of the effective origin, Δ_o, can be incorporated into the model using Equations (2) and (16).

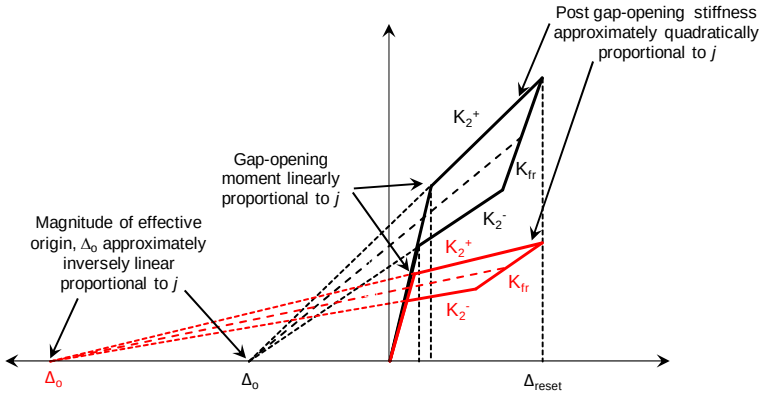

Fig. 4 Representation of the dependence of the effective origin, Δ_o on the fractional lever-arm, j.

4.1 Model Implementation

The overall tangent stiffness is defined as K_t, and incorporates the model developed within the previous sections, accounting for elastic beam and column flexibility and the contributions from the rigid body rotations and tendon behaviour, defined in Equations (10) to (15). Note that this model includes the modifications presented to account for friction, yielding, prestress reduction or loss, and overall connection behaviour and directional dependence. The tangent stiffness can therefore be used in a time-incremental formulation to relate input column displacement, Δ, to connection moment and thus, column shear.

4.2 Experimental Validation

The experimental corner joint configuration presented in Li et al.[2] and Rodgers[7] utilising a bent tendon profile was chosen for experimental validation. This configuration presents very complex overall hysteretic response that captures almost all of the considerations presented in the model development. The experimental specimen had basic dimensions, defined in Figure 1, of $L_{col} = 2.9$m, $h_{col} = 0.7$m, $L = 4$m, $L_b = 3.65$m, and $D = 0.56$m. In the experiment, for positive joint rotations, $j_{PT}^{+} = 0.66$, and $D = 560$mm so that $(jD)_{PT}^{+} = 370$ mm, and for negative joint rotations, $j_{PT}^{-} = 0.34$ so that $(jD)_{PT}^{-} = 190$mm.

5. Results and Discussion

The test specimen underwent quasi-static uni-directional displacement tests in the seismic direction using fully reversed sine wave profiles up to 4% inter-story drift. The experimental data for the exterior connection was utilized as it is the most difficult case to model due to the asymmetry in gap opening force, friction, and yield displacement. An interior connection of this type, with two beams present was also tested, but is not used for comparison. The interior connection was symmetrical, and although the tendons were non-centrally located, the overall joint exhibited symmetrical hysteretic behavior. The reason for this observation is that the two connections are undergoing opposite rotations, and the asymmetry from the non-central location of the tendons is balanced by the opposing connection. Therefore, the exterior connection is the most stringent test of the model, and once validated can be extended to also model the interior joint if desired. Figure 5 presents the experimental and model results for the subassembly.

Overall, very good agreement is evident between the computational model and the experimental results. The subassembly shows very good agreement, and captures the tendon yield, friction, and loss of prestress following large response cycles causing tendon yield.

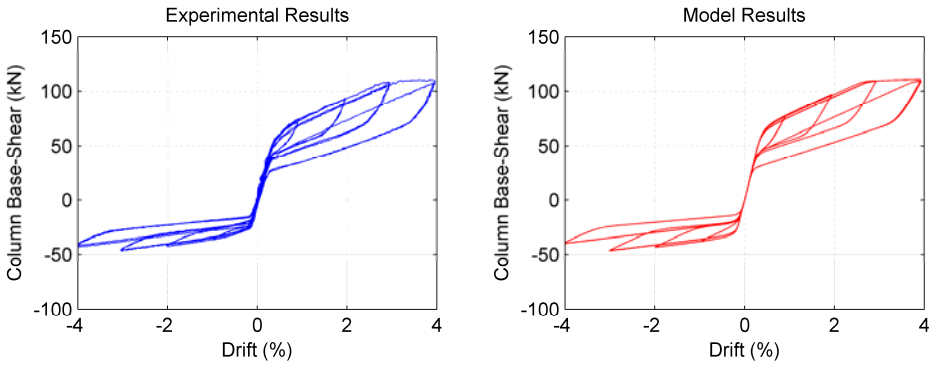

Fig. 5 Experimental and model results

6. Summary

The advanced analytical model of joint hysteresis using a compound, time-incremental Menegotto-Pinto and Ramberg-Osgood model shows very good agreement to experimental results. The ability to accurately predict the entire hysteretic response of the connection at any drift level is an important outcome for analysis purposes. Overall, this model is more complex and harder to implement than the simpler explicit forms in previous research. However, this model provides a much more robust description. If any significant friction or tendon yield is likely to occur then the simpler explicit models will no longer provide accurate results. The presence of friction, yielding and prestress reduction are all modelled accurately, providing good overall agreement. Finally, this model is not intended for initial design, but as an analysis tool. This model could be incorporated into a commercial or open source analysis program as a reliable means of modelling a jointed precast connection.

References

(1) L. Li, Further Experiments on Damage Avoidance design of Beam-to-column joints, in *Dept. of Civil Engineering*. 2006, University of Canterbury: Christchurch, New Zealand.
(2) L. Li, J.B. Mander, and R.P. Dhakal, Bi-Directional Cyclic Loading Experiment on a 3-D Beam-Column Joint Designed for Damage Avoidance. ASCE Journal of Structural Engineering, 2008. Vol. 134(11): pp. 1733-1742.
(3) M.J.N. Priestley, S. Sritharan, J.R. Conley, and S. Pampanin, Preliminary results and conclusions from the PRESSS five-story precast concrete test building. PCI Journal, 1999. Vol. 44(6): pp. 42-67.
(4) K.M. Solberg, Experimental and financial investigations into the further development of damage avoidance design, in *Department of Civil Engineering*. 2007, University of Canterbury: Christchurch, New Zealand.
(5) J.B. Mander, Beyond ductility: The quest goes on. Bulletin of the New Zealand Society for Earthquake Engineering, 2004. Vol. 37(1): pp. 35-44.
(6) G.W. Rodgers, K.M. Solberg, J.B. Mander, J.G. Chase, B.A. Bradley, R.P. Dhakal, and L. Li, Performance Of A Damage-Protected Beam-Column Subassembly Utilizing External HF2V Energy Dissipation Devices. Earthquake Engineering & Structural Dynamics, 2008. Vol. 37(13): pp. 1549-1564.
(7) G.W. Rodgers, Next Generation Structural Technologies: Implementing High Force-To-Volume Energy Absorbers, in *Dept. of Mechanical Engineering*. 2009, University of Canterbury: Chirstchurch, New Zealand.
(8) M. Menegotto and P. Pinto. "Method of analysis for cyclically loaded reinforced concrete plane frames including changes in geometry and non-elastic behavior of elements under combined normal force and bending.". in IABSE Symposium on the Resistance and Ultimate Deformability of Structures Acted on by Well-defined Repeated Loads,. 1973. Lisbon.
(9) W. Ramberg and W.R. Osgood, Description of Stress-strain Curves by Three Parameters. National Advisory Committee on Aeronautics, Technical Note 902, 1943.

Acknowledgements

This work was developed while the first author was at Texas A&M University on a Fulbright-EQC Graduate Award. The support of Fulbright New Zealand, the Earthquake Commission, and the Tertiary Education Commission is gratefully acknowledged.